Pergamon

Int. J. Heat Mass Transfer. Vol. 38, No. 7, pp. 1151–1159, 1995

0017-9310/95 $9.50+0.00

0017-9310(94)00246-0

Effect of model orientation and wall heating condition on local heat transfer in a rotating two-pass square channel with rib turbulators

JAMES A. PARSONS, JE-CHIN HAN† and YUMING ZHANG

Turbine Heat Transfer Laboratory, Department of Mechanical Engineering, Texas A&M University, College Station, TX 77843-3123, U.S.A.

(*Received* 13 *December* 1993 *and in final form* 28 *July* 1994)

Abstract—The influences of channel orientation and wall heating condition on the local surface heat transfer coefficient in a rotating, two-pass, square channel with 60° and 90° ribs on the leading and trailing walls were investigated for Reynolds numbers from 2500 to 25 000 and rotation numbers from 0 to 0.352. The two channel orientations were (1) square channel perpendicular to the axis of rotation and (2) square channel twisted at 45° to the axis of rotation. Two thermal boundary condition cases were studied: (A) all four walls at the same temperature and (B) all four walls at the same heat flux. Results show the Coriolis force effect is reduced for the 45° channel orientation. Thus, heat transfer coefficients decrease for the first pass trailing and second pass leading walls and increase for the first pass leading and second pass trailing walls, compared with their corresponding perpendicular channel orientation values. The increase of heat transfer coefficients for uneven wall heating condition Case (B) when compared to their corresponding heat transfer coefficients for Case A is greater for the 45° channel orientation than for the perpendicular channel orientation.

INTRODUCTION

As turbine inlet temperature increases in gas turbine engines so does the heat load to the turbine blades. To maintain acceptable blade life, methods such as film cooling, impingement cooling, and augmented convective cooling in internal serpentine and pin fin channels reduce the amount of heat reaching the blades and remove the heat from the blades. Some investigations for the heat transfer in internal coolant channels of turbine blades have concentrated on non-rotating models that did not include the Coriolis and the centrifugal buoyancy forces effect on coolant motion and heat transfer [1, 2]. However, some researchers reported on the heat transfer characteristics due to rotation in straight channels with smooth or rib turbulated walls and radial outward flow [3–9]. References [10–13] studied the effect of rotation on the local heat transfer coefficient in a serpentine square coolant channel (three-pass) with smooth and ribbed walls for a systematic variation of parameters similar to typical engine conditions. References [14, 15] also showed results for rotation effects on the local heat transfer coefficient but in a four-pass smooth and ribbed square channel. Reference [16] predicted the channel fluid velocities and heat transfer coefficients in rotating smooth channels with radial outward flow, which agreed within 10–30% with the smooth wall data shown in ref. [10].

References [17–20] present the effect of wall heating condition on local heat transfer coefficients in a two-pass square channel with smooth and rib turbulated walls. The results of refs. [17, 18] agreed with those of refs. [10, 11] for the rotating smooth wall channel with uniform wall temperature conditions, i.e. all walls at the same temperature. However, refs. [17–20] found that for the uniform wall heat flux and simulated engine wall heating conditions, the rotating leading surface heat transfer coefficients of the first coolant pass (radial outward flow) and the rotating trailing surface heat transfer coefficients of the second coolant pass (radial inward flow) were 50–100% greater than those for the uniform wall temperature conditions.

Many of the above used coolant channel walls perpendicular to the axis (or direction) of rotation with radial outward (and inward) flow. However, Figs. 1 and 2 show that the orientation of the cooling channel in the leading and trailing edge regions of the turbine blade may be at an angle β to the axis of rotation. Reference [21] recently investigated the effect of channel orientation for uniform wall temperature conditions. Since the wall heating condition significantly affects heat transfer for rib turbulated surfaces [19, 20] of a rotating channel, it is unknown how effects due to wall heating condition change when these channel walls are at an angle β to the axis of rotation for both radial outward and inward flow. Therefore, this study will investigate the effects of channel orientation and wall heating condition on local surface heat transfer coefficients in a rotating two-pass square channel with 60° and 90° ribs on the leading and trailing walls. Two channel orientations are studied: $\beta = 0°$ corresponding to the mid-portion of a turbine blade (data from refs. [19, 20]), and

† Author to whom correspondence should be addressed.

NOMENCLATURE

A	projected heat transfer surface area
D	hydraulic diameter; square channel width or height (= 0.0127 m, 0.50 in.)
e	rib height
h	heat transfer coefficient
k	thermal conductivity of coolant (air)
L	heated channel length (each pass)
Nu	local Nusselt number, hD/k
Nu_o	Nusselt number in stationary, fully developed, turbulent, tube flow
P	rib pitch or streamwise spacing
Pr	Prandtl number
q_{net}	net heat transfer rate
$\bar{R}$	mean rotating radius
Re	Reynolds number, $\rho DV/\mu$
Ro	rotation number, $\Omega D/V$
T_b	local bulk mean coolant temperature
T_{bi}	inlet bulk mean coolant temperature
T_w	local wall temperature
V	mean coolant channel velocity
X	channel axial distance from heated channel inlet
X'	channel axial distance from second pass inlet.

Greek symbols

α	the angle between the coolant flow direction and the rib axis
β	channel (or model) orientation angle
$(\Delta\rho/\rho)_i$	coolant-to-wall density ratio based on inlet bulk mean coolant temperature, $(\rho_{bi}-\rho_w)/\rho_{bi} = (T_w-T_{bi})/T_w$
Ω	rotational speed
ρ	coolant density
ρ_{bi}	coolant density based on inlet bulk mean coolant temperature
ρ_w	coolant density based on local wall temperature
μ	coolant dynamic viscosity.

$\beta = 45°$ corresponding to serpentine passages in the trailing edge region of a blade (new data) (Fig. 1). The two wall heating conditions tested were Case A (four walls at the same temperature) and Case B (four walls at the same heat flux).

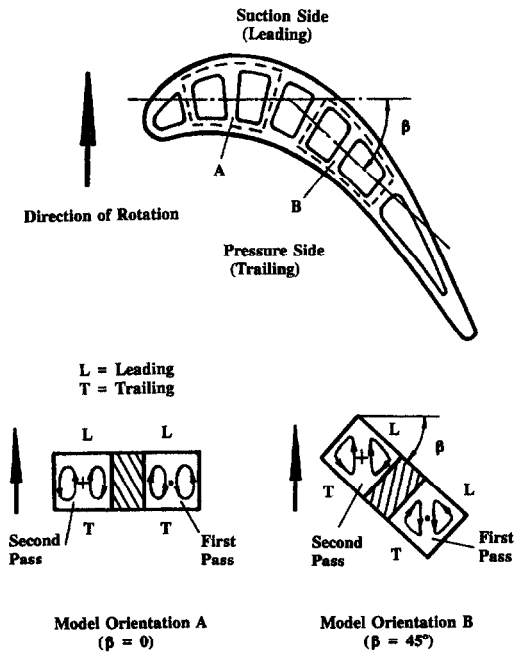

Fig. 1. Coolant channel orientations and cross-stream flows in a turbine blade.

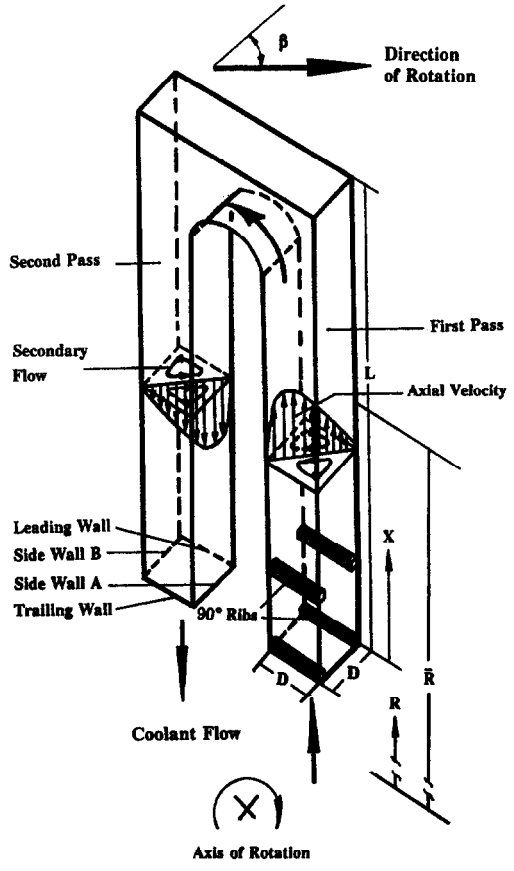

Fig. 2. Conceptual view of the coolant flow profile and 90° transverse ribs in a twisted two-pass rotating channel.

EXPERIMENTAL FACILITY AND DATA REDUCTION

References [17–20] describe the test rig, test procedures, data reduction and uncertainty. A short description follows; Fig. 3(a). Regulated, compressed air (coolant) flows through an orifice meter and passes through a hollow rotating shaft and a hollow rotating arm perpendicularly mounted onto the shaft. Then the air passes through the test model (a ribbed, two-pass, square channel at the outer radius of the arm), is routed back to the shaft and exits into the atmosphere from the opposite end of the rotating shaft. Slip ring units transfer thermocouple outputs to a data logger interfaced to a personal computer and also transfer variac transformer outputs to wire resistance heaters uniformly cemented in grooves on the backside of the test model's copper plates. The front sides of the copper plates form the channel walls. Each plate is isolated in the streamwise and circumferential directions by Teflon pieces of the test model. The plates serve to obtain regionally averaged heat transfer coefficients; Fig. 3(b). An electric motor with an adjustable frequency controller turns the shaft, arm, and test model by means of a toothed belt. A digital photo tachometer measures the rotating shaft speed.

The arm, the unheated entrance channel, and test model twist about the long axis of the rotating arm to achieve the two channel orientations. For the $\beta = 45°$ orientation (twisted), the ribbed leading wall for the $\beta = 0°$ orientation (untwisted) and smooth side wall A become co-leading walls (Figs. 1 and 2). Similarly, the ribbed trailing wall and smooth side wall B become co-trailing walls. The ribbed leading and trailing walls back against the suction and pressure surfaces of the blade, respectively, for both untwisted and twisted orientations, and are the main walls of interest. Figure 2 shows that ribs are directly opposite each other (not staggered) on both leading and trailing walls. As in previous studies, the rib height-to-hydraulic diameter ratio (e/D) is 0.125, the rib pitch-to-height ratio (P/e) is 10, and the rib angle from the coolant flow direction (α) is 90° (Fig. 2) or 60°; Fig. 3(b). The ribbed trailing and leading surfaces are made by gluing brass ribs of square cross-section to the copper plates. The thickness of the conductive glue is less than 0.01 cm and creates a negligible thermal insulation effect between the ribs and copper plates.

Calculation of the local heat transfer coefficient uses the local net heat transfer rate, the projected surface area (area of the smooth wall) to the cooling air, the local wall temperature on each copper plate, and the local bulk mean air temperature in

$$h = q_{net}/[A(T_w - T_b)]. \quad (1)$$

Local net heat transfer rate (q_{net}) is the electrical power generated by the heaters minus the power loss by conduction away from the channel. The local bulk mean air temperature uses the corresponding X/L (or X'/L) for each thermocouple location in interpolating between the measured inlet (about 30°C) and exit bulk temperatures. The local Nusselt number, normalized by the Nusselt number for a stationary fully developed turbulent flow in a smooth circular tube, is correlated

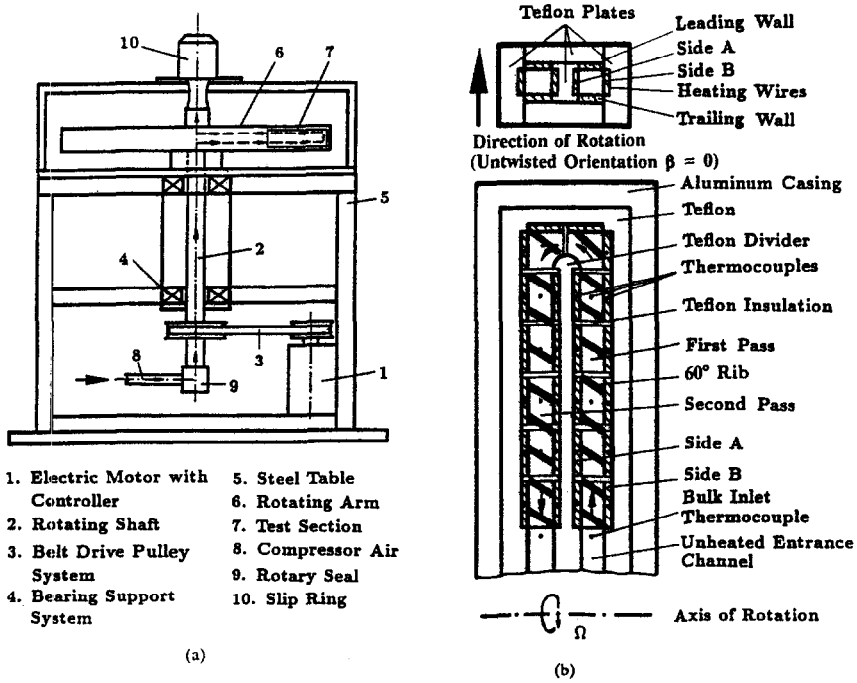

Fig. 3. (a) Schematic of the rotating test rig and (b) Schematic of the heat transfer test model with +60° angled ribs for an untwisted two-pass rotating channel.

by Dittus–Boelter/McAdams [22] as

$$Nu/Nu_0 = (hD/k)/[0.023\,Re^{0.8}\,Pr^{0.4}] \quad (2)$$

with $Pr = 0.72$. The uncertainty of the local heat transfer coefficient depends on the local wall-to-coolant temperature difference and the net heat input to the coolant for each copper plate. This uncertainty increases when decreasing both the local wall-to-coolant temperature difference and the net heat input. Considering the method described in ref. [23], the typical uncertainty in the Nusselt number is estimated to be less than 8% for Reynolds numbers greater than 10 000. The maximum uncertainty, however, could be up to 20–25% for the lower heat transfer coefficient at the lowest Reynolds number tested ($Re = 2500$).

EXPERIMENTAL RESULTS AND DISCUSSION

Along with what refs. [12, 19] show, the Nusselt number in a rotating channel is also a function of the channel geometry. Thus, the Nusselt number depends on: (1) the ratio of the rotating mean radius to channel hydraulic diameter, (2) the ratio of the axial distance to channel hydraulic diameter, (3) channel Reynolds number, (4) Prandtl number, (5) rotation number, (6) wall-to-coolant density (temperature) difference ratio, (7) flow direction (radial outward flow or radial inward flow), (8) rib turbulator geometry (height, spacing, cross-section, and angle between the coolant flow direction and the rib axis, respectively) and (9) the channel geometry (shape and orientation). The functional relationship can be expressed as:

$$Nu = f(\bar{R}/D, X/D, Re, Pr, Ro, \Delta\rho/\rho,$$

flow direction, rib geometry, channel geometry) (3)

where $Pr = 0.72$ and $\bar{R}/D = 30$. Results are shown for the following test conditions: $Re = 2500$, 5000, 10 000 and 25 000 and $\Omega = 0$ and 800 rpm, which combine to produce $Ro = 0.0$, 0.0352, 0.088, 0.176 and 0.352. The inlet wall-to-coolant density ratio $(\Delta\rho/\rho)_i$ has the following values: Case A = 0.11 for all walls in both passes (producing $T_w = 60$–65°C) and Case B = 0.10, 0.07 and 0.08 for the first pass leading ($T_w = 60$–65°C), trailing ($T_w = 50$–55°C) and two side walls ($T_w = 55$–60°C), respectively (the reverse is true for the second pass leading and trailing walls).

Effect of rotation relative to non-rotation

Figures 4 and 5 show the effect of rotation ($Ro = 0$, 0.0352 and 0.176) on the local Nusselt number ratio (Nu/Nu_0) for 90° transverse ribs on the leading and trailing walls, Case A wall heating condition, and for both untwisted and twisted channel orientations. In Fig. 4 for $Ro = 0$ and 0.176 at $Re = 5000$, local Nusselt number ratios for the ribbed leading and trailing walls are nearly uniform for non-rotation (approximately 2.5–4.5) throughout the two-pass test model. However, as rotation increases ($Ro = 0$–0.176), in the first outward flow pass ($0 < X/D < 12$) the Nusselt

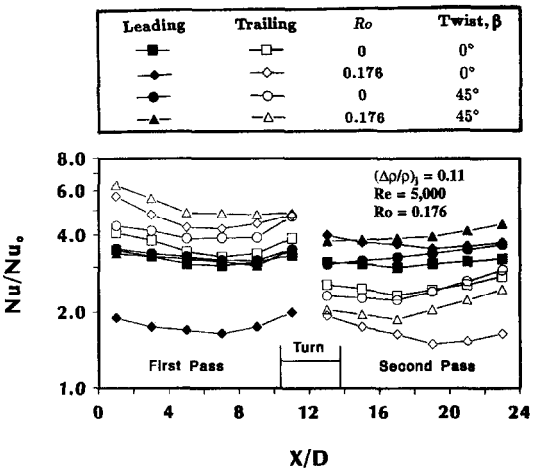

Fig. 4. Effect of rotation on Nusselt number ratio variation for Case A, 90° ribs, $Ro = 0$, 0.176 and $\beta = 0°$, 45°.

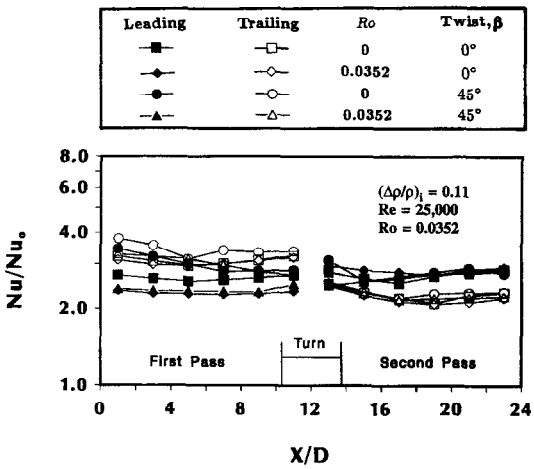

Fig. 5. Effect of rotation on Nusselt number ratio variation for Case A, 90° ribs, $Ro = 0$, 0.0352 and $\beta = 0°$, 45°.

number ratios for the trailing wall increase while the Nusselt number ratios for the leading wall decrease relative to their corresponding non-rotating values. The reverse is true in the second inflow pass ($12 < X/D < 24$). This is because rotation creates Coriolis forces, proportional to the through flow velocity, which produce secondary, cross-stream flows. Figure 1 shows these flows impinge perpendicularly on the first pass trailing and second pass leading walls for the untwisted model orientation A ($\beta = 0°$). Similarly, these cross-stream flows for the twisted model orientation B ($\beta = 45°$) still impinge on the first pass trailing and second pass leading walls but at an oblique angle β. Thus, not only do these cross-stream flows thin the boundary layers of the first pass trailing and second pass leading walls, but the fluid is also pulled away from, and thus thickens the boundary layers on the first pass leading and second pass trailing walls. Therefore, due to the thinning or thickening of the boundary layers, the heat transfer coefficients for

both the untwisted and twisted orientations for the first pass trailing and second pass leading walls are higher with rotation than those without. The heat transfer coefficients for the first pass leading and second pass trailing walls are also lower with rotation than those without. However, the Coriolis force effects and cross-stream flows are reduced as rotation number is reduced. Figure 5 shows smaller differences between Nusselt number ratios for rotation number $Ro = 0.0352$ (at $Re = 25\,000$) and their corresponding Nusselt number ratios for non-rotation ($Ro = 0$) compared to the differences between Nusselt number ratios for rotation number $Ro = 0.176$ (at $Re = 5000$) and non-rotation in Fig. 4.

Effects of rotation number, channel orientation and wall heating condition

Before these new results are presented and discussed, a brief summary follows of the untwisted channel orientation results from refs. [19, 20]. For Cases A and B wall heating conditions, the Nusselt number ratios for the first pass trailing wall increase with increasing rotation number and are higher than the Nusselt number ratios for the first pass leading wall, which decrease with increasing rotation number. The reverse is true for the second pass. The magnitude of the differences between the leading and trailing Nusselt number ratios in both passes increase with increasing rotation number. However, these differences are reduced in the second pass when compared to the first pass differences. This is because the rotation induced centrifugal buoyancy force (radially outward and due to air density–temperature differences) adds to the inertia force in the first pass and subtracts from the inertia force in the second pass. Thus, the through flow velocity and Coriolis force effect (explained above) are reduced in the second pass when compared to the first pass. Therefore, the magnitude of the leading–trailing Nusselt number differences are smaller in the second pass.

Figures 6, 7, 9 and 10 show the effects of channel orientation and rotation number on Nusselt number ratio for the following wall heating condition–rib angle combinations: Case A, 90° transverse rib (Fig. 6); Case A, 60° angled rib (Fig. 7); Case B, 90° transverse rib (Fig. 9); and Case B, 60° angled rib (Fig. 10). Results are presented at four selected channel axial locations: $X/D = 7$ and 11 in the first outward flow pass, and $X/D = 13$ and 17 (or for X', $X'/D = 1$ and 5) in the second inward flow pass. First, Figs. 6 and 7 for Case A uniform wall temperature will be discussed. The twisted orientation, 60° angled rib results for Case A will then be compared to the results in ref. [21]. Finally, Figs. 9 and 10 for Case B uniform wall heat flux will be discussed.

Both Figs. 6 and 7 show results for Case A 90° and 60° ribs, respectively. The Nusselt number ratios for the first pass and second pass trailing walls for the twisted orientation are nearly equal to those Nusselt number ratios corresponding to the untwisted model

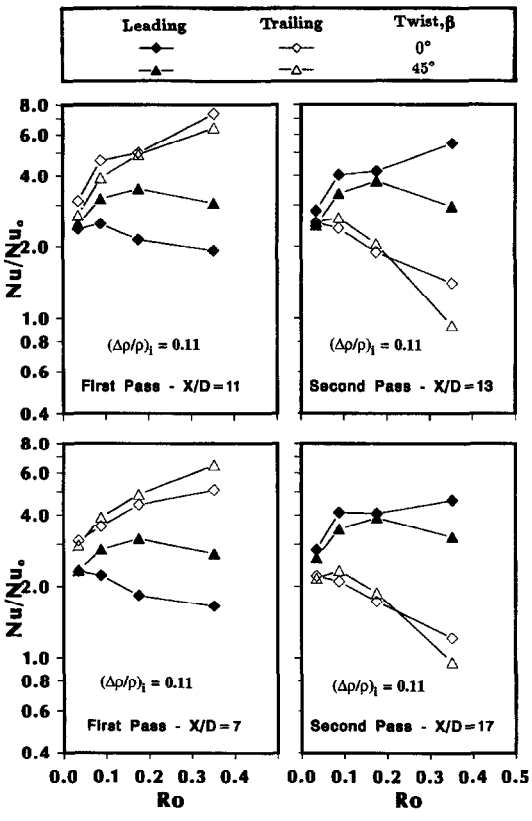

Fig. 6. Effect of rotation number on Nusselt number ratio variation at selected axial locations for Case A, 90° ribs and $\beta = 0°, 45°$.

orientation. The Nusselt number ratios for the twisted orientation of the first pass leading wall are up to 120% higher and about 40% lower for the second pass leading wall, respectively, than those Nusselt number ratios for the untwisted orientation. This may be explained as follows. The effect of the Coriolis force for the untwisted orientation is a maximum since these forces (and cross-stream flows) are normally incident on the first pass trailing and second pass leading walls. This produces maximum differences between leading and trailing Nusselt number ratios in each pass. However, the Coriolis force effect (and cross-stream flows) are still present for the twisted orientation but reduced by being oblique at 45° to the first pass trailing and second pass leading walls (Fig. 1). Thus, the increases (decreases) of the Nusselt number ratios for the first pass trailing and second pass leading (first pass leading and second pass trailing) walls from non-rotating results are not as great for the twisted orientation as for the corresponding increases (decreases) for the untwisted orientation. This is the effect of model orientation on the Coriolis force (and cross-stream flow).

Note that the amount of change (increase) in the Nusselt number ratios for the first pass leading wall, which occurs as the orientation changes from untwisted to twisted, are relatively greater than the

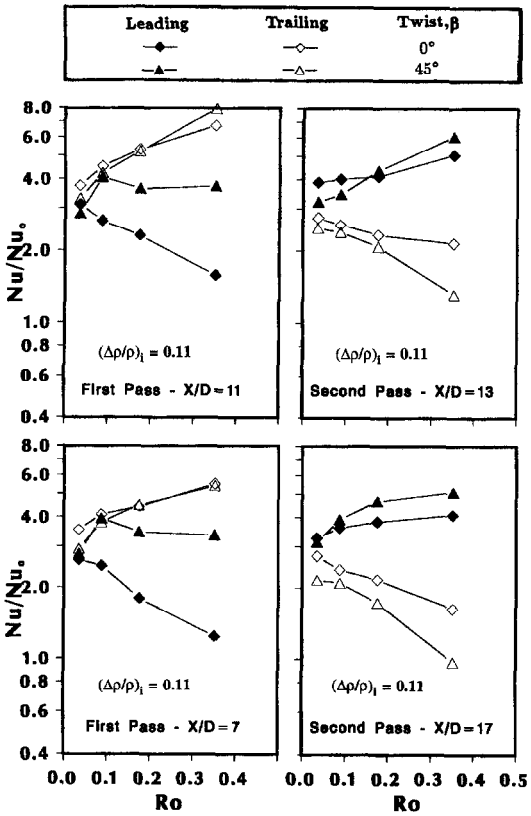

Fig. 7. Effect of rotation number on Nusselt number ratio variation at selected axial locations for Case A, 60° angled ribs and $\beta = 0°, 45°$.

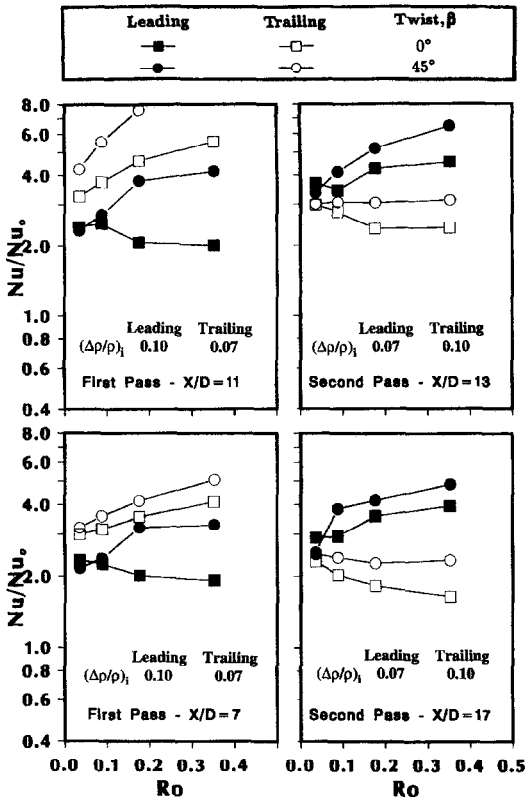

Fig. 9. Effect of rotation number on Nusselt number ratio variation at selected axial locations for Case B, 90° ribs and $\beta = 0°, 45°$.

amount of change for any of the other three walls. The Coriolis and the buoyancy forces for the untwisted orientation pull fluid away from almost the entire width of the first pass leading wall, which creates a relatively thick boundary layer on the first pass leading wall. For the twisted orientation, however, these

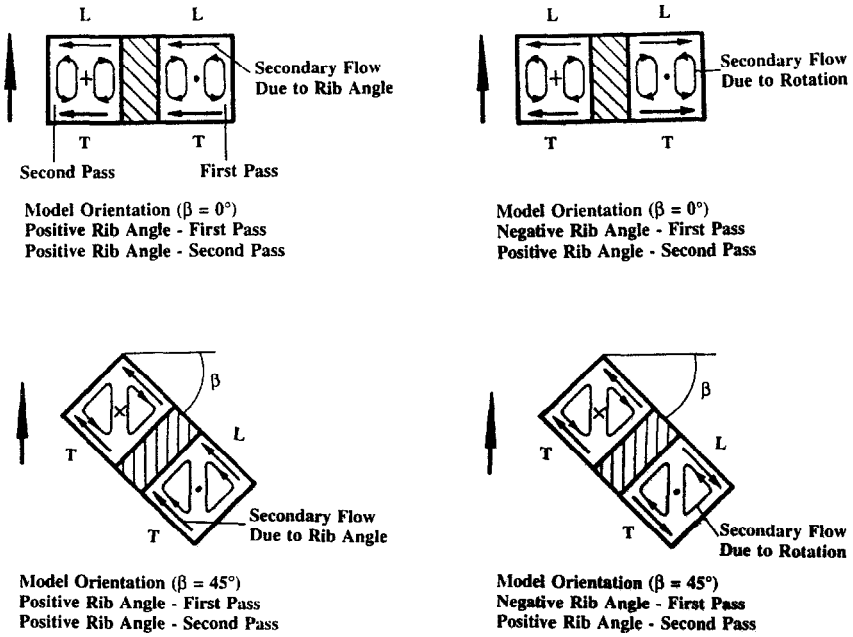

Fig. 8. Conceptual view of secondary flow vortices induced by rotation, model orientation and rib angle.

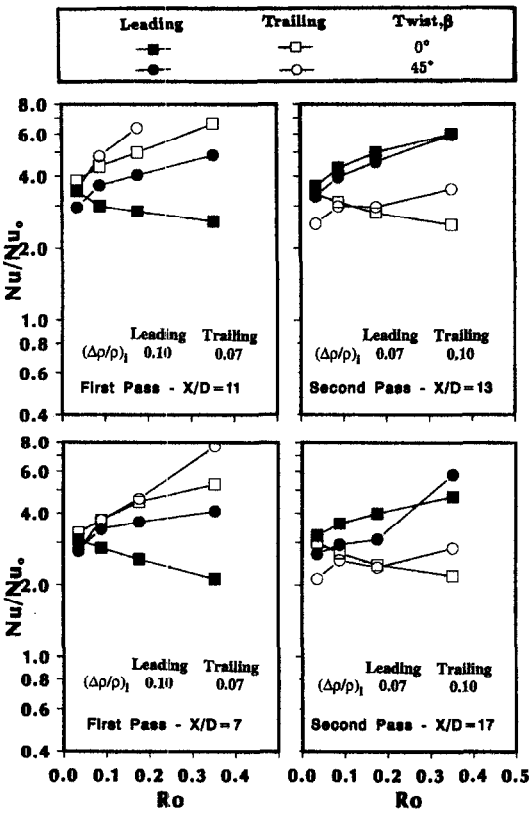

Fig. 10. Effect of rotation number on Nusselt number ratio variation at selected axial locations for Case B, 60° angled ribs and $\beta = 0°, 45°$.

forces only pull fluid away from the part of the wall nearest the corner of the leading wall and side wall A (Figs. 1 and 2). Thus, the boundary layer on the leading wall for the twisted orientation remains relatively thin (increases Nusselt number ratios). The boundary layers for the first pass trailing wall are already thin and not significantly affected by the reduction in Coriolis force as the model orientation changes. However, the amount of change (decrease) in the Nusselt number ratios for the second pass leading wall is smaller as the orientation changes, compared to the change (increase) for the first pass leading wall.

Figure 7 shows the effect of model orientation on Nusselt number ratios for Case A uniform wall temperature and 60° angled ribs. As mentioned above, ref. [21] also presents local heat transfer results for rotating, square-cross section, serpentine passages with ribbed walls. The pertinent data in ref. [21] are identified as uniform wall temperature, 45° angled (skewed) rib, model orientation at +45°, and forward flowing coolant for the trailing edge region of a turbine blade (positive rotation). The 45° angled ribs in ref. [21] are shorter in height ($e/D = 0.1$) and semi-circular in cross section but, most importantly, are at a rib angle of $\alpha = -45°$ (or $\alpha = +135°$) from the coolant flow direction in the first pass (radial outward flow) and at $\alpha = +45°$ in the second pass (radial inward flow), compared to the rib angle of $\alpha = +60°$ in both passes for the present data (Fig. 3(b)).

The results of ref. [21] for the +45° angled ribs in the second, inward flow pass agree with the present data for +60° angled ribs: small differences between the Nusselt number ratios for the untwisted and twisted model orientations for both the leading and trailing walls. However, for the first pass with −45° angled ribs, the Nusselt number ratios for the trailing wall decrease and remain about the same for the leading wall as the model orientation changes from untwisted to twisted ($\beta = 0°$ to $-45°$), which is different from the present study results. Here Fig. 7 shows that the Nusselt number ratios for +60° angled ribs in the first pass for the trailing wall remain about the same but increase greatly for the leading wall as model orientation changes from untwisted to twisted.

Part of the explanation follows. Along with the secondary cross-stream flow produced by the Coriolis force effect, another secondary flow along the rib axes is produced solely by the effect of ribs at an angle, but not transverse, to the coolant flow direction [2]. It makes no difference if the rib angle is positive or negative for stationary tests with full width ribs and regional heat transfer measurements using full width copper plates. It is also believed there is no difference due to the sense of the rib angle for the rotating untwisted model orientation results [13, 19, 20]. This is because the two secondary flows produced by the Coriolis force and rib angle effects combine to (i) constructively (same direction) enhance heat transfer for one half of each of the leading and trailing walls and (ii) destructively (opposite direction) reduce heat transfer for the other half of each of the leading and trailing walls for either positive or negative angled ribs. This can be seen from the conceptual secondary flow diagrams in Fig. 8 (upper diagrams). However, the two secondary flows for the rotating twisted model orientation (see Fig. 8 lower diagrams) combine to (i) constructively (same direction) enhance heat transfer for positive rib angles on both leading and trailing walls in the first pass and (ii) destructively (opposite direction) reduce heat transfer for negative rib angles on both leading and trailing walls in the first pass. Therefore, changing the model orientation from untwisted to twisted, the heat transfer on *both leading and trailing walls*: increases for +60° angled ribs in the first pass but decreases for the −45° angled ribs in the first pass. This is the effect of the combined Coriolis force and rib angle on the secondary cross-stream flows.

The other part of the explanation is the effect of model orientation on Coriolis force, mentioned above for Figs. 6 and 7. Combining all effects (Coriolis force, rib angle, and model orientation on secondary flows shown in Fig. 8), explains the results in the first pass as model orientation changes from untwisted to twisted for ref. [21] with −45° angled ribs, and for the present data with +60° angled ribs. The first pass heat transfer for the −45° angled ribs trailing wall

decreases due to the reduced Coriolis force effect and the opposite direction between rib angle and the model orientation effect on secondary vortices. However, heat transfer for the leading wall remains about the same because the enhanced Coriolis force effect cancels the opposite direction between rib angle and the model orientation effect on secondary vortices. The first pass heat transfer for the $+60°$ angled ribs trailing wall remains about the same due to cancellation of the reduced Coriolis force effect with the positive rib angle and the model orientation effect on secondary vortices. The leading wall increases due to combination of the enhanced Coriolis force effect with the positive rib angle and the model orientation effect on secondary vortices. It is interesting that there is no secondary flow for 90° transverse ribs due to rib angle and thus, the model orientation effect on secondary flow dominates this situation.

Finally, Figs. 9 and 10 for 90° and 60° ribs, respectively, show results for Case B uniform wall heat flux. Many of the Nusselt number ratios on both leading and trailing walls for the twisted model orientation Case B could be up to 100% above those Nusselt number ratios corresponding to the untwisted model orientation. Again, the most significant increases (up to 100%) occur on the first pass leading wall, the same as the Case A results. The effect of model orientation on the Coriolis force (and cross-stream flow) clearly increases heat transfer for the first pass leading and second pass trailing walls as explained above for Figs. 6 and 7. However, the results for the 60° angled ribs on the second pass are insensitive to model orientation. This could be due to the very complicated flow situation (i.e. 60° angled ribs, twisted model orientation, uneven wall heating condition, and flow exiting the sharp 180° turn). The reasons for the increases of the first pass trailing wall and the 90° rib second pass leading wall when the model twists under uneven wall heating conditions are explained below.

For the untwisted orientation, the flow in the two secondary cross-stream flow vortices is heated in the boundary layers of three walls: the leading wall, trailing wall, and one of the two side walls (model orientation A, Fig. 1). The temperature of the first pass leading wall is higher than the other walls for the first pass and uniform wall heat flux. However, the twisted orientation flow in each secondary cross-stream flow vortex is now heated either by the leading wall or the trailing wall and by one of the two side walls (model orientation B, Fig. 1). Thus, the twisted orientation cross-stream flow vortex next to the trailing wall and one side wall no longer has heating at the relatively warm leading wall as the corresponding vortex did for the untwisted orientation. Therefore, the flow next to the trailing wall for the twisted orientation is relatively cooler than the untwisted orientation. Thus heat transfer and Nusselt number ratios significantly increase for the first pass trailing wall (and similarly for the second pass leading wall) and overcome the effect of the model orientation to decrease heat transfer on these two walls. Significant Nusselt number increases (relative to Case A) were also found for untwisted model orientations that were due to uneven wall heating conditions [17–20].

Several additional comparisons can be made on Figs. 6, 7, 9 and 10 and are briefly stated below. Nusselt number ratios for the untwisted orientation 60° and 90° ribs (referred to as ratios) on both leading and both trailing walls of Case B vary from 20% below to 50% above their corresponding ratios for Case A. However, twisted orientation ratios for both leading and both trailing walls of Case B vary from 25% below to 150% above their corresponding ratios for Case A. Thus, the twisted orientation generally increases the effect of uneven wall heating, when compared to the smaller increases in heat transfer due to uneven wall heating condition for the untwisted orientation. In addition, the untwisted orientation ratios for the 60° angled ribs on both leading and both trailing walls are up to 30% above their corresponding ratios for both Cases A and B 90° ribs. However, the twisted orientation ratios for the 60° angled ribs on both leading and both trailing walls for Case A are up to 40% above and for Case B are within 40% of their corresponding ratios for the 90° ribs. Finally, Figs. 6, 7, 9, and 10 show changes in Nusselt number ratios as the model orientation changes from untwisted to twisted up to 120% for the leading and trailing walls of the first pass and only up to 40% for the leading and trailing walls of the second pass. The smaller changes in the second pass are due to the reduction of the inertia force by the buoyancy force in the second pass.

CONCLUDING REMARKS

The influences of channel orientation to the axis of rotation and wall heating condition on the local surface heat transfer coefficients in a rotating, two-pass, square channel with 60° and 90° ribs on the leading and the trailing walls have been observed for rotating numbers from 0.0 to 0.352 and Reynolds numbers from 2500 to 25 000. The findings are:

1. The effects of the Coriolis force and cross-stream flow reduce as the model orientation changes from untwisted (channel walls perpendicular to the axis of rotation) to twisted (channel walls at 45° to the axis of rotation). Thus, the Nusselt number ratios for the twisted first pass trailing and second pass leading walls are reduced when compared to their corresponding Nusselt number ratios for the untwisted orientation. The Nusselt number ratios for the twisted first pass leading and the second pass trailing walls are also enhanced when compared to their corresponding Nusselt number ratios for the untwisted orientation. The largest change is the enhancement of up to 120% (Case A) on the first pass leading wall.

2. Nusselt number ratios for the untwisted orientation 60° and 90° ribs on both leading and both

trailing walls for Case B (uniform wall heat flux condition) vary from 20% below to 50% above their corresponding Nusselt number ratios for Case A (uniform wall temperature condition). However, Nusselt number ratios for the twisted orientation 60° and 90° ribs on both leading and both trailing walls of Case B vary from 25% below to 150% above their corresponding Nusselt number ratios for Case A. Thus, the effect of uneven wall heating condition (Case B) is greater (and generally increases) for the twisted orientation than for the untwisted orientation. This is due in part to the change in the number of walls that heat the coolant in the cross-stream flow vortices of the channel which occurs as the model orientation changes. Also, the greatest increase is up to 100% on the first pass leading wall.

3. The Nusselt number ratios for the untwisted orientation and both Cases A and B 60° ribs on both leading and both trailing walls are up to 30% above their corresponding Nusselt number ratios for the 90° rib walls. However, the Nusselt number ratios for the twisted orientation 60° ribs on both leading and both trailing walls for Case A are up to 40% above, while Case B are within 40% of their corresponding Nusselt number ratios for the 90° rib walls.

Acknowledgement—The Texas Higher Education Coordinating Board-Energy Research in Application Programs supported this investigation: Project Number 999903-050, TEES 70730.

REFERENCES

1. J. C. Han, Heat transfer and friction in channels with two opposite rib-roughened walls, *ASME J. Heat Transfer* **106,** 774–781 (1984).
2. J. C. Han and J. S. Park, Developing heat transfer in rectangular channels with rib turbulators, *Int. J. Heat Mass Transfer* **31,** 183–195 (1988).
3. Y. Mori, T. Fukada and W. Nakayama, Convective heat transfer in a rotating radial circular pipe (2nd report), *Int. J. Heat Mass Transfer* **14,** 1807–1824 (1971).
4. R. J. Clifford, W. D. Morris and S. P. Harasgama, An experimental study of local and mean heat transfer in a triangular-sectioned duct rotating the orthogonal mode, *ASME J. Engng Gas Turbines Pwr* **106,** 661–667 (1984).
5. S. P. Harasgama and W. D. Morris, The influence of rotation on the heat transfer characteristics of circular, triangular, and square-sectioned coolant passages of gas turbine rotor blades, *ASME J. Turbomachinery* **110,** 44–50 (1988).
6. J. Guidez, Study of the convective heat transfer in rotating coolant channels, *ASME J. Turbomachinery* **111,** 43–50 (1989).
7. C. Y. Soong, S. T. Lin and G. J. Hwang, An experimental study of convective heat transfer in radially rotating rectangular ducts, *ASME J. Heat Transfer* **113,** 604–611 (1991).
8. M. E. Taslim, A. Rahman and S. D. Spring, An experimental investigation of heat transfer coefficients in a spanwise rotating channel with two opposite rib-roughened walls, *ASME J. Turbomachinery* **113,** 74–82 (1991).
9. M. E. Taslim, L. A. Bondi and D. M. Kercher, An experimental investigation of heat transfer in an orthogonally rotating channel roughened with 45 degree criss-cross ribs on two opposite walls, *ASME J. Turbomachinery* **113,** 346–353 (1991).
10. J. H. Wagner, B. V. Johnson and T. J. Hajek, Heat transfer in rotating passages with smooth walls and radial outward flow, *ASME J. Turbomachinery* **113,** 42–51 (1991).
11. J. H. Wagner, B. V. Johnson and F. C. Kopper, Heat transfer in rotating serpentine passages with smooth walls, *ASME J. Turbomachinery* **113,** 321–330 (1991).
12. J. H. Wagner, B. V. Johnson, R. A. Graziani and F. C. Yeh, Heat transfer in rotating serpentine passages with trips normal to the flow, *ASME J. Turbomachinery* **114,** 847–857 (1992).
13. B. V. Johnson, J. H. Wagner, G. D. Steuber and F. C. Yeh, Heat transfer in rotating serpentine passages with trips skewed to the flow, *ASME J. Turbomachinery* **116,** 113–123 (1994).
14. W. J. Yang, N. Zhang and J. Chiou, Local heat transfer in a rotating serpentine flow passage, *ASME J. Heat Transfer* **114,** 354–361 (1992).
15. N. Zhang, J. Chiou, S. Fann and W. J. Yang, Local heat transfer distribution in a rotating serpentine rib-roughened flow passage, *ASME J. Heat Transfer* **115,** 560–567 (1993).
16. C. Prakash and R. Zerkle, Prediction of turbulent flow and heat transfer in a radially rotating square duct, *ASME J. Turbomachinery* **114,** 835–846 (1992).
17. J. C. Han and Y. M. Zhang, Effect of uneven wall temperature on local heat transfer in a rotating square channel with smooth walls and radial outward flow, *ASME J. Heat Transfer* **114,** 850–858 (1992).
18. J. C. Han, Y. M. Zhang and K. Kalkuehler, Uneven wall temperature effect on local heat transfer in a rotating two-pass square channel with smooth walls, *ASME J. Heat Transfer* **115,** 912–920 (1993).
19. Y. M. Zhang, J. C. Han, J. A. Parsons and C. P. Lee, Surface heating effect on local heat transfer in a rotating two-pass square channel with 60° angled rib turbulators, *ASME J. Turbomachinery*, accepted (1995).
20. J. A. Parsons, J. C. Han and Y. M. Zhang, Wall heating effect on local heat transfer in a rotating two-pass square channel with 90° rib turbulators, *Int. J. Heat Mass Transfer* **37,** 1411–1420 (1994).
21. B. V. Johnson, J. H. Wagner, G. D. Steuber and F. C. Yeh, Heat transfer in rotating serpentine passages with selected model orientations for smooth or skewed trip walls, *ASME J. Turbomachinery* **116,** 738–744 (1994).
22. W. M. Rohsenow and H. Choi, *Heat, Mass and Momentum Transfer*, pp. 192–193. Prentice-Hall, Englewood Cliffs, NJ, U.S.A. (1961).
23. S. J. Kline and F. A. McClintock, Describing uncertainties in single-sample experiments, *Mech. Engng* **75,** 3–8 (1953).